



Tides and tidal currents in the Pearl River Estuary

Qingwen Mao^{a,*}, Ping Shi^a, Kedong Yin^{a,b}, Jianping Gan^b, Yiquan Qi^a

^aKey Laboratory of Tropical Marine Environmental Dynamics (LED), South China Sea Institute of Oceanology, Chinese Academy of Sciences, 164 West Xinggan Road, Guangzhou, China

^bAtmospheric, Marine & Coastal Environment (AMCE) Program, Hong Kong University of Science and Technology, Clear Water Bay, Kowloon, Hong Kong SAR, Hong Kong

Received 28 April 2003; accepted 28 March 2004

Available online 10 August 2004

Abstract

Several cruises were conducted to investigate the variability in tidal levels, tidal flows, and water circulation in the Pearl River estuary during the dry and wet seasons in 1998. Unlike other temperate estuaries, the average tidal range was small in the offshore waters and increased gradually towards the estuary, reaching the maximum in the upstream part of the Pearl River estuary. The extent of the amplitude increment was different between the diurnal and semi-diurnal constituents. The percentage of sea level variance in the semi-diurnal band increased when the tide progressed upstream, but it reversed in the diurnal band. Thus, the accentuated sea level variance in the semi-diurnal band resulted in the increased amplitudes of semi-diurnal constituents which were larger than diurnal constituents. The distribution of the mean current in the estuary depicted an anti-clockwise circulation in the estuary: freshwater was dominant on the western side of the estuary, while salt water was dominant on the eastern side. The Pearl River estuary also showed a typical salt wedge circulation: a salt water intrusion largely occurred via the eastern channel in the estuary while river outflow dominated the western channel. In this study, long time series and large spatial coverage of tide and current observations allow in depth analysis of the temporal and spatial variations of tide and circulation, and the associated influence from open ocean in the Pearl River estuary.

© 2004 Elsevier Ltd. All rights reserved.

Keywords: Pearl River Estuary; Tidal cycles; Tidal ranges; Tidal asymmetry; Tidal flows; Water circulation

1. Introduction

Estuaries can be characterized by their geomorphology and their pattern of salinity stratification (Hansen and Rattray, 1966). In coastal plain

estuaries, the vertical distribution of salinity is regulated primarily by the volume of freshwater outflow and the magnitude of the tidal current (Leonard, 1976). The constant mixing between freshwater and seawater results in a variable environment in estuaries. Numerous physical factors including the volume of river discharge, intensity of tidal action, tidal currents and

*Corresponding author.

E-mail address: qwmao@scsio.ac.cn (Q. Mao).

elevations, the composition of the sediments, and wind and wave energy contribute to the overall complexity of these coastal environments. The interaction of river flow, tidal currents, and basin morphology produces the type of circulation and related salinity structure characteristic of a particular estuary that affects the species composition and distribution of flora and fauna.

Tides are the periodic rise and fall of the sea level due to attractive forces of the sun, moon, and earth. Tides and tidal currents are a major source of energy for turbulence and mixing in estuaries and they play an important role in the movement of dissolved and particulate material, creating oscillatory fluxes in physical and chemical properties. The dissipation of tidal energy causes changes in the vertical stability of the water column. Denman and Powell (1984) showed that tidal mixing is important for phytoplankton and primary productivity because it produces light and nutrient fluctuations. Yin et al. (1995a, b) showed that the tidal-regulated estuarine circulation played an important role in entrainment of nutrients and phytoplankton seed populations in the Fraser River estuary and adjacent coastal waters of the Strait of Georgia (Canada).

The Pearl River Estuary (PRE, Fig. 1), connected with the Pearl River at its northern end, is situated in the southern China (Guangdong Province). The shape of the PRE is like an inverted funnel with the narrow neck in the north and wide mouth opening to the south. The width of the PRE is about 4 km at the northern end near Humen and about 60 km between Lantau Island (Hong Kong) and Macau at the southern end. The length of the PRE is about 63 km between the two ends. The area within the inverted funnel is also known as Lingdingyang in Chinese. In this paper, we will refer to it as the PRE. The topography of the PRE has mixed features of channels, shoals and tidal flats (Fig. 1). The depth of the estuary varies from 0 to 30 m. Freshwater discharges from the four river mouths located in the northwest side of the PRE where water depths are between 2 and 5 m. Humen is one of the river mouths at the northern end of the PRE. There are two deep

channels along the PRE. The east channel has a water depth of about 10 m and the west channel is shallower. These geographic and topographic features exert dynamic influences on tidal cycles, water circulation and the water column structure and consequently, they affect water quality and estuarine ecosystems.

The tides in the PRE mainly come from the Pacific oceanic tidal propagation through the Luzon Strait (Ye and Preiffer, 1990) with a mean tidal range between 1.0 and 1.7 m. They are also influenced by the geometry and bottom topography, meteorological factors and river discharge. There have been large-scale field observations on tides and tidal currents in the PRE in the past and numerous tidal charts have been produced for this region based on these measurements. These charts display the co-tidal and co-range lines of the principal semi-diurnal (M2 and S2) and diurnal (K1 and O1) tides. M2 is usually the dominant semi-diurnal tidal constituent, followed by K1, O1, and S2. The (K1 + O1)/M2 constituent amplitude ratio has been used to indicate the tidal pattern, and the ratio in the PRE ranges from 0.94 at Humen, to 1.77 at Wanshan Islands, south of Hong Kong (Zhao, 1990). Thus the tidal cycle in this area is mainly a semi-diurnal mixed tidal regime with daily inequality in range and time between the highs and lows. More significant daily inequality is found in the southern part of the Lingdingyang. With the tidal wave progressing upstream, the tidal energy is concentrated and the tidal range is amplified because of the inverted funnel shape topography. In the cross-estuary section, there is a significant difference in tidal ranges between the east and west sides with larger tidal ranges in the east (Xu, 1985; Zhao, 1990). To the north of Nei Ling Ding Island, the currents are rectilinear current, but to the south of Nei Ling Ding Island the currents are rectilinear in the channel and rotary in the shallow waters. Extensive tidal modeling studies have also been performed (Ye and Preiffer, 1990; Shaoling and Kot, 1997). Ye and Preiffer (1990), using both analytical and three-dimensional numerical models, concluded that incident and reflected Kelvin tidal waves are formed because the estuary is wide enough to induce a significant Coriolis effect. The

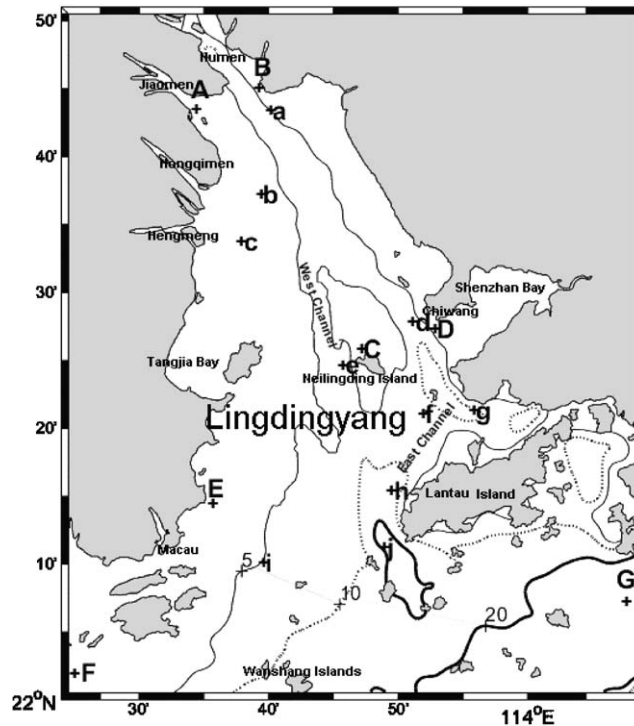


Fig. 1. Topography of the PRE with the 5 (thin solid line), 10 (dashed) and 20 m (thick solid line) isobaths shown. The location of stations for the tidal gauges (Stns A–G) and for current velocity measurements (Stns a–j) are shown. Stn. H is located 20 km east of Stn G.

pattern of residual currents in the PRE is counter-clockwise resulting from stronger flood currents on the east side and stronger ebb currents on the west side. Due to rapid economic growth in the Pearl River delta region, there have been many projects along the shoreline and in the estuary, such as building harbors, navigation dredging and sand dredging, and land reclamation. These projects have changed the shoreline and the topography of the estuary and thus, produced impacts on the water flow and sediment transport in the estuary. There have been concerns with how the local hydrodynamics have been modified due to various projects in the surrounding area of the PRE.

The objective of this study was to characterize variations in the tidal levels, and tidal velocity and to examine how the estuarine circulation is related to tidal cycles during the dry and wet seasons based on these observations.

2. Data and methods

Sampling stations for tidal gauges were set up in the upstream part of the PRE (Stns A and B), the middle eastern part (Stns C and D), western part (Stn E) (Fig. 1). Stns F, G and H were outside the estuary, with Stn F on the west side and Stns G and H on the east side (Stn H, 20 km east of Stn G, not shown in Fig. 1), respectively. Sampling stations for current velocities were distributed in the upstream (Stns a, b, and c), the mid-eastern (Stns e, d, f, and g), the western (Stn i) and eastern parts (Stns h and j) as shown in Fig. 1.

Field measurements of tides and currents were obtained during cruises in March, June, July, September and November 1998 (Table 1). The dates for the duration of tidal and velocity measurements for each site are given in Table 1. Hourly tidal level data were collected at Stn C for a period of one month at three time intervals: July

Table 1
Stations for tidal gauges and current measurements and duration of observations during 1998

Current stations	Duration (dd.mm)	Tidal stations	Duration (dd.mm)
a, f	09.03–24.03 01.07–16.07	A, C, D, F, H	20.07–20.08 11.09–11.10 07.11–07.12
b, c, g, j	11.03–12.03 19.03–20.03 04.07–05.07 09.07–10.07	B E	19.06–20.07 20.06–20.07
d, e, h, i	24.07–26.07 25.09–27.09 22.11–24.11	G	22.02–29.03

20–August 20, September 11–October 11, and November 7–December 7. Tidal level data were continuously recorded every 10 min at Stns B, E and G for a period of more than 30 days. The current data at Stns E and B were collected with a WLR-7 (Aanderaa Ltd.) and data at Stn B were obtained with an S4-ADW (Inter-Ocean). The hourly tide records at Stns A D, F and H (Fig. 1, H located 20 km east of G) from 7 November to 7 December 1998 were obtained from the South China Sea Branch, State Oceanic Administration (SOA, China). All tidal records were converted to the data above the Hong Kong Principal Datum.

Vertical profiles of current speed and direction at Stns a and f (Fig. 1) were recorded and lasted for half a month with a Nortek ADP-1500 mounted on the sediment bottom. At other stations, the current profiles, using hand-held DRCM SLC 9-2 current meters deployed from a boat, were obtained in different locations in the estuary during the tidal cycle survey. At these stations, the hourly current measurements were recorded for 26 h at Stns b, c, g, j and for 22 h at Stns d, e, h, I, respectively.

Analysis of the data extract the amplitudes and phases of major tidal constituents from both sea surface elevation and velocity records. The tidal height data at each tidal station and current data measured by ADP were analyzed with tidal computer software (Foreman, 1978) which uses a least squares analysis method incorporating nodal modulation astronomical argument correction, and inference calculations for the amplitudes and

phases. There is a maximum of 146 possible tidal constituents that can be included in the tidal analysis: 45 of these are astronomical in origin (equilibrium tidal constituents), while the remaining 101 are shallow water constituents. As the length of the current records at other stations were insufficient to resolve M2 and S2, O1 and K1, the most important semi-diurnal and diurnal constituents were obtained by applying quasi-harmonic tidal analysis.

3. Results and discussion

3.1. Variability in sea level

Figs. 2 and 3 demonstrate that tidal cycles were mixed semi-diurnal tides in both PRE (Stn A) and offshore waters (Stn H) with daily inequality. Larger ebb ranges occurred after higher high waters. This daily inequality in tidal ranges increased gradually as tidal ranges increased. The largest daily inequality occurred in spring tides during Julian days 203–205 in the wet season and 324–327 in the dry season. In general, tidal ranges during both ebb and flood tides were smaller at the offshore station H where daily tidal inequality was more significant. Based on the average tidal range of <2 m, the PRE can be classified as a microtidal estuary. The tidal duration was also asymmetrical over a daily tidal cycle as it was in-phase with the tidal range inequality (Figs. 2 and 3). Thus, a larger tidal range corresponded to a longer tidal

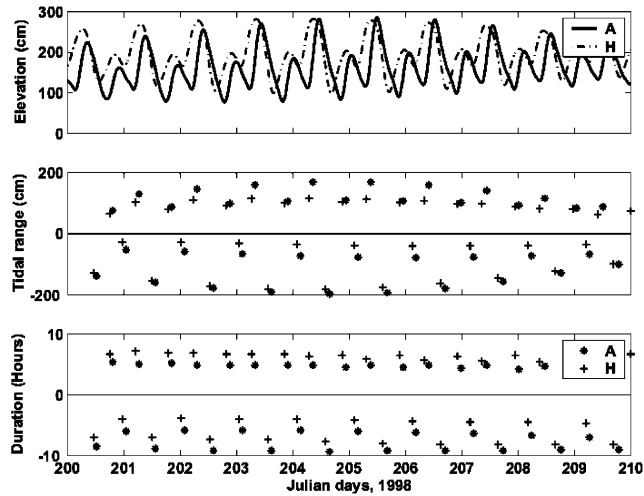


Fig. 2. Tidal cycle, tidal range and tidal duration at Stns A and H in the wet season. Negative values in the tidal range and tidal duration indicate the ebb range and ebb duration, respectively.

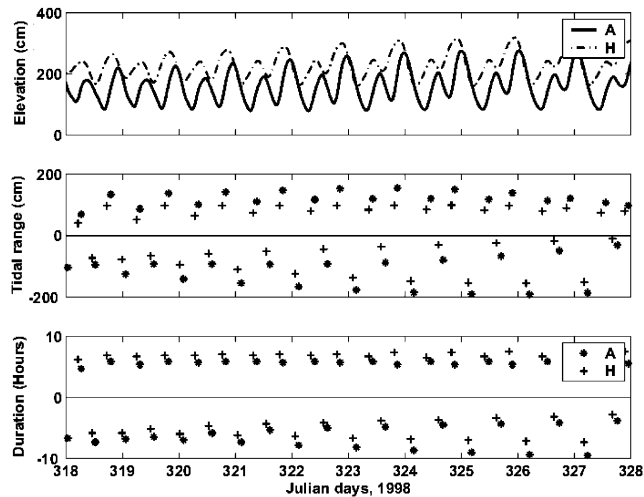


Fig. 3. The same as in Fig. 2 except for the dry season.

duration. The duration of an ebb tide was longer than a flood tide and the largest ebb duration occurred during spring tides. This indicates that when the tidal wave propagated from offshore into the PRE, the speed of the trough of a wave was retarded more than the crest near the shallow bottom in the PRE. Qualitatively similar tidal characters were found between the wet and dry seasons at both Stn A and H. During the wet

season, the increased river discharge increased the ebb duration towards the lower low water.

Tidal amplitudes and Greenwich phases for the main individual constituents are given in Table 2. In the Lindingyang, the M2 constituent had the largest amplitude for each of the tidal gauge records, followed by K1, O1 and S2 (Fig. 4). The M2 amplitude was the highest at Stn B, near Humen (the river mouth), reaching 63.6 cm. At

Table 2

Amplitudes (*a*) and phase angles (*g*) of the significant tidal constituents for the Pearl River Estuary by harmonic analysis of the sea level data in 1998 including the wet and dry seasons

Tide	Stations															
	A		B		C		D		E		F		G		H	
	<i>a</i>	<i>g</i>														
MSF	8.4	74	10.9	48	7.1	95	5.5	85	6.7	53	5.9	97	1.7	150	5.1	85
O ₁	25.4	290	27.8	288	31.3	259	32.0	257	30.2	256	29.9	253	28.6	246	27.9	248
K ₁	31.0	340	45.7	339	38.5	312	39.2	308	48.4	312	35.9	304	23.8	310	33.5	300
N ₂	9.1	338	8.0	321	11.0	288	11.9	283	8.1	266	9.3	266	7.4	244	7.4	255
M ₂	49.7	348	63.6	331	56.5	303	59.8	299	51.4	286	45.8	279	33.2	254	35.5	266
S ₂	18.2	17	15.6	2	23.0	332	23.2	330	15.1	322	18.5	309	16.9	290	14.0	292
M ₄	4.1	245	9.3	198	2.8	91	3.7	83	4.9	61	3.6	56	6.9	279	3.2	307
S ₄	0.1	23	0.1	53	0.1	294	0.0	31	0.2	127	0.1	117	0.5	305	0.1	21
MS ₄	2.6	291	3.2	265	1.6	133	1.9	120	1.6	110	2.0	104	4.5	348	2.1	354
M ₆	1.2	82	1.9	62	0.6	237	0.5	254	1.3	220	0.5	241	2.4	97	0.5	124
M ₈	0.3	296	0.4	230	0.2	351	0.0	69	0.2	239	0.3	261	0.1	45	0.2	72
2g _{M2} -g _{M4}		91		94		155		155		151		142		229		203

a: Amplitude (centimeters); *g*: Phases (degrees).

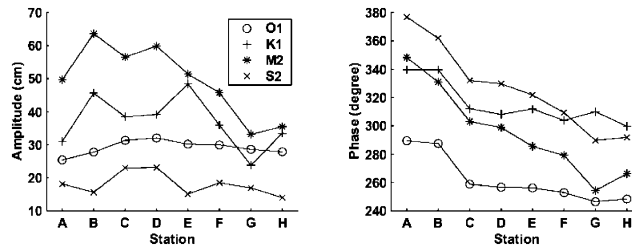


Fig. 4. The amplitudes and phases for dominant semi-diurnal M2, S2 and dominant diurnal K1, O1 at stations with tidal gauges in the Pearl River estuary.

Stns G and H, the amplitudes for O1, K1 and M2 were comparable. In general, the equilibrium diurnal and semi-diurnal tides decayed within the estuary, through both friction and non-linear transfers of energy (Aubrey and Speer, 1985; Speer and Aubrey, 1985). Friction at the water-sediment interface usually reduces the amplitude of the tides and creates a phase lag. However, this was not the case in the PRE as shown in Fig. 4. The M2 amplitude increased from the offshore (Stn H) to the northern end of the Lindingyang by approximately 80%, and the phase lag for M2 was approximately 90° (3 h). The amplitudes of K1, O1 and S2 also increased from the offshore to the estuary, but the amplitude of O1 decreased in the northern part of the PRE. Thus, the mean tidal

range increased gradually from the offshore into the estuary. The phase lag of S2 was similar to M2 with a magnitude of about 90°. Unlike the dominant semi-diurnal tides with a gradual delay in the phase from offshore to the PRE, the phase lag for the dominant diurnal tides (O1 and K1) was weak in the southern part and suddenly increased in the northern part of the PRE.

Sea level variance (SLV) distribution is another important property of tides. Since the sampling times at Stns A, C, D, F, and H were identical, the results of the frequency band distribution of sea level variance at these stations were selected and summarized in Table 3. The percentage of sea level variance in the semi-diurnal band increased from offshore to the estuary, but it reversed for the

Table 3
Percentage of sea level variance in the different frequency bands

Stns	Low-Frequency Band % $f < 0.025$ cph	Diurnal Band % $0.025 < f < 0.05$ cph	Semi-diurnal Band % $0.05 < f < 0.1$ cph	High-Frequency Band % $f > 0.1$ cph
A	5.2	29.3	61.4	4.0
C	3.7	32.4	62.8	1.1
D	2.6	31.2	64.9	1.2
F	5.0	37.9	55.5	1.5
H	4.1	46.6	47.7	1.6

(f : frequency, cph: cycles per hour).

diurnal band. At an offshore Stn H, the average semi-diurnal SLV was 47.7% and the average diurnal SLV was 46.6% and hence the percentage of SLV in the semi-diurnal and diurnal bands was comparable at this station. In the central part of the estuary (Stn D), the average semi-diurnal SLV reached 64.9% while the average diurnal SLV was only 31.2%, indicating that SLV in diurnal band was significantly attenuated within the PRE and SLV in the semi-diurnal band was accentuated from offshore to the estuary. The percentage of SLV in the high-frequency band was accentuated at Stn A, while the values were comparable in other stations. In the low-frequency band, the percentage of energy was comparable at all stations. The accentuated SLV in the semi-diurnal band resulted in increased amplitudes of the semi-diurnal constituents which were larger than the diurnal constituents. Therefore, the (K1 + O1)/M2 constituent amplitude ratio was reduced gradually when the tide propagated into the PRE. In the northwest part of the estuary, very shallow waters and a large area of tidal flats (Fig. 1) might attribute to a large decay of amplitude, a longer phase lag both in the diurnal band and semi-diurnal band, and a significant accentuation in the high-frequency band at Stn A.

Tidal asymmetry in which the duration of the ebb tide was longer than the flood tide, was an important feature in Lindinyang except for the southeastern end. The tidal asymmetry exerts effects on both the geological evolution of shallow estuaries and the navigability of estuarine channels. An estuary characterized by shorter, more intense flood than ebb currents (flood dominant) may be unable to flush sediments in the estuary

effectively. Conversely, an estuary with stronger ebb than flood currents (ebb dominant) may maintain a more stable configuration (Aubrey and Speer, 1985; Friedrichs and Aubrey, 1988). In semi-diurnal tidal regimes, the flood- or ebb-dominance is considered to be governed by the phase relationship between the M2 and M4 constituents given by $2g_{M2} - g_{M4}$, where g_{M2} and g_{M4} are the phase lags of M2 and M4 constituents, respectively. The result of M4 phase leading to M2 is a distorted surface tide with falling tides exceeding rising tides in duration (Aubrey and Speer, 1985). Aubrey showed that estuarine currents are: (1) flood-dominant when $90^\circ < 2g_{M2} - g_{M4} < 270^\circ$; and (2) ebb-dominant when $-90^\circ < 2g_{M2} - g_{M4} < 90^\circ$. The last row of Table 2 gives the value of $2g_{M2} - g_{M4}$ at each station. In the PRE, the ranges of $2g_{M2} - g_{M4}$ were between 90° and 270° , and thus the PRE was characterized by shorter, more intense flood than ebb currents (flood dominant). Within Lindinyang, the duration asymmetry due to the M2–M4 interaction became more pronounced far away from shallow areas with extensive flats. It reached extreme values in the northwest part of the estuary where the difference between the ebb and flood duration was about 2.5 h (Figs. 2 and 3). The sediment transported from river runoff in western the PRE cannot be flushed out of the estuary due to the flood dominance and it forms the large area of flats in the western part of the PRE. The tidal duration differences varied significantly with the season. The average differences were small in winter and larger in summer (Fig. 5). The largest difference occurred in July (2.8 h) and the smallest difference in October (1 h). These results agreed

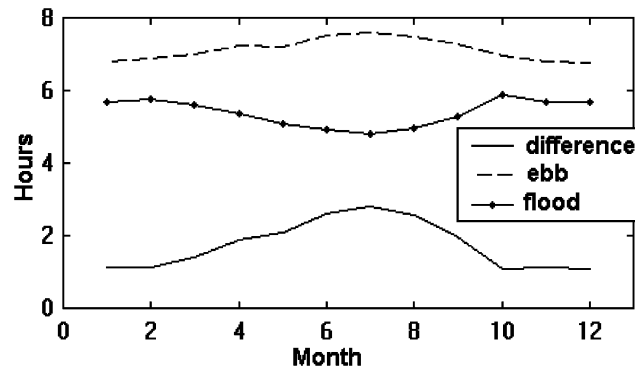


Fig. 5. Monthly average flood duration, ebb duration and the differences between the two (using 1959–1983 historical sea level data) at Hengmen.

with a previous study (Xu, 1985), which indicated that the flood-to-ebb duration ratio increased smoothly downstream and eastward, and the tidal duration asymmetry was strongly dependent on the river discharge: the large river discharge in the wet season increases the ebb duration (Xu, 1985).

3.2. Tidal flows and circulation

The scatter plots of the end-point of the top and bottom layer's current vectors for the 10 available records at the current stations (Stns a–j) during the dry season and wet season are shown in Figs. 6 and 7, respectively. The water flow was dominated by the northwest–southeast direction at most stations except for Stn f where the current direction was mostly along the east–west axis. The ebb tidal currents flowed southwards to the mouth of the estuary. In general, currents at the surface were stronger than at the bottom.

In the north and central parts of Lindingyang (Stns a–f), the mean currents at both the surface and bottom were directed southward toward the mouth of the estuary, indicating that the river discharge created a dominant flow for the non-tidal current in the estuary. In the northwestern part of the PRE, there are four river inlets, and as a result, the mean currents were always stronger in the northwest than in the northeast part of Lindingyang. In the wet season, a larger river discharge causes more intense mean currents than in the dry season. At Stn c, the mean current velocity was 63 cm s^{-1} at the surface and 48 cm s^{-1}

at the bottom in the wet season (Fig. 7), which were the maximum mean currents in the PRE. In the southeast part of Lindingyang (Stns g, h, j), the mean current directions were always reversed between the surface and bottom. The mean flows showed that the surface was dominated by the river discharge while the current at the bottom was dominated by the seawater intrusion into the Lindingyang and formed the salt wedge estuarine circulation. The maximum salt water intrusion occurred near the bottom at Stn g where the mean currents reached 26 cm s^{-1} . Thus, the seawater intrusion appeared to flow largely through the eastern channel as its main channel in Lindingyang, while the freshwater outflow used the western channel as its main pathway. The finding is consistent with the general pattern described previously (Zhao, 1990). A larger vertical velocity shear was found in the wet season in Stns. G, h and j as the result of stronger river discharge.

The results of the harmonic analysis of the current data are shown in Fig. 8. They depicted the current ellipses and the direction of the rotation for the dominant semi-diurnal M2, S2 and the dominant diurnal K1, O1 at the three measurement layers of all current stations. The inclinations of the ellipses at most stations are in the northwest-southeast direction except for Stns f, h and i. The eccentricity of the tidal current ellipses was small and there were few eccentricities larger than 0.2. Therefore, the tidal currents in Lindingyang were almost rectilinear. The maps (Fig. 8) depicted the direction of the tidal rotation when

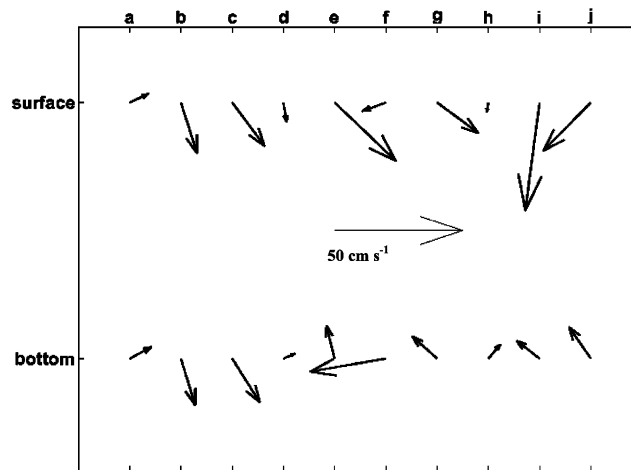


Fig. 6. Mean velocity vectors (cm s^{-1}) at the surface and bottom obtained from the current meter moorings in the dry season. The letters in the x-axis indicate the mooring stations. The plots are characterized in three groups. Stns a–c are located at northern part of the PRE, and stns d–g are located at central part of the PRE, while stns h–j are located at south part of the PRE.

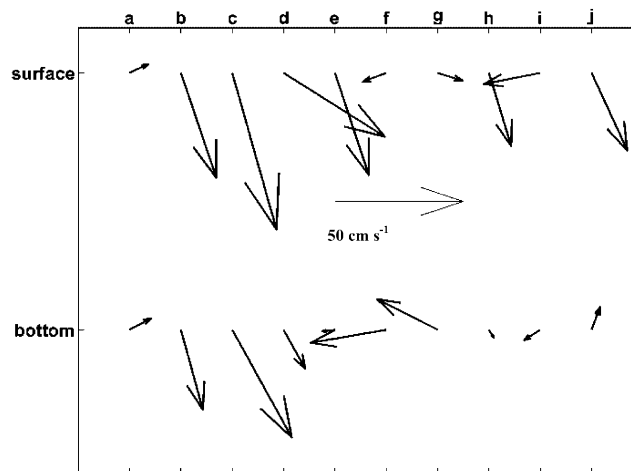


Fig. 7. The same as in Fig. 6 except for the wet season.

the eccentricity was larger than 0.1. Generally, the major axis of the M2 tidal current ellipse was about twice as large as that of O1, K1 and S2 constituents. The major axes of dominant diurnal constituents K1 and O1 at Stn a were small in comparison with other stations.

The combined effects of ellipse parameters of the dominant semi-diurnal M2, S2 and dominant diurnal K1, and O1 constituents could be best visualized by presenting snapshots of the predicted

tidal currents (Andreas, 1998). Fig. 9 mapped the tidal currents in the upper layer at four different phases for one sea level oscillation cycle. At the time of the low water at Stn B (at point 0 in Fig. 9a), the tidal flow direction was out of the estuary at the top end of the estuary, while it was into the estuary in other regions (Fig. 9b). Tidal currents were larger in the east than in the west, which was consistent with previous observations (Xu, 1985). During the rising tide (at point 1 in

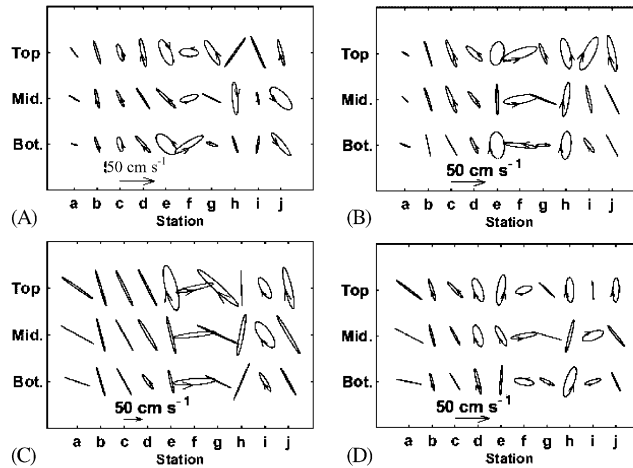


Fig. 8. The tidal current ellipses in three layers (top, middle and bottom in y-axis) for each current station (x-axis) for individual tidal constituents (A) O1, (B) K1, (C) M2, (D) S2.

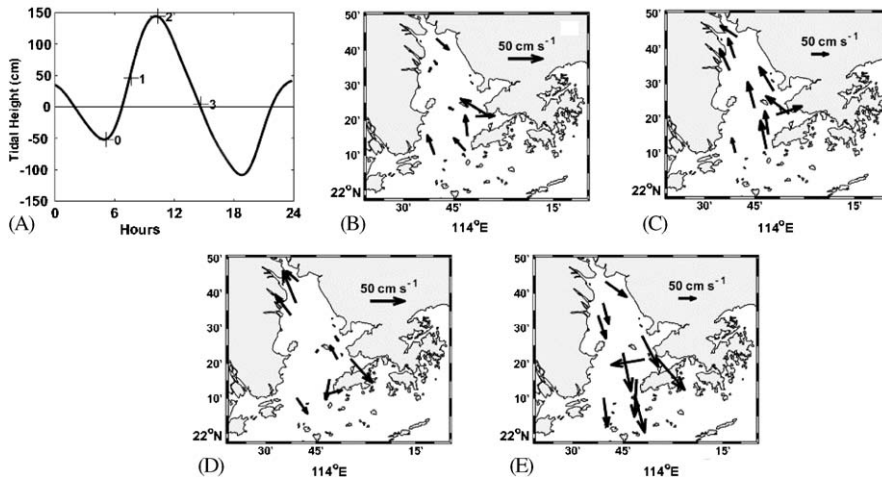


Fig. 9. Tidal currents predicted from dominant semi-diurnal M2, S2 and dominant diurnal O1, K1 tidal ellipse parameters for July 9, 1998. Graph (A) Tidal levels at Stns B; Graphs (B), (C), (D) and (E) depict tidal currents for times 0, 1, 2, 3 denoted in (A).

Fig. 9a), the tidal currents progressively flowed into the estuary from the mouth of the estuary and the stronger flood velocities of 90 cm s⁻¹ were found in the east channel. At Stn f, tidal flow was eastward, while at the other stations tidal flow was northward. When the sea level reached the higher high water (at point 2 in Fig. 9a), southwestward flowing currents developed from the mouth of the estuary toward the end of the estuary (Fig. 9d). In the middle of the ebb tide, (at point 3 in Fig. 9a),

all currents flowed out of the estuary and reached a maximum ebb velocity of about 100 cm s⁻¹ (Fig. 9e).

By combining the effect of ellipse parameters of the dominant semi-diurnal M2, S2 and dominant diurnal K1, O1, the predicted tidal currents during several tidal cycles were also presented. Figs. 10 and 11 show the variability of predicted tidal current speeds and vectors at Stns c, g and j during both the dry and wet seasons, respectively. In the northern and central parts of the PRE (Stns c and g), the

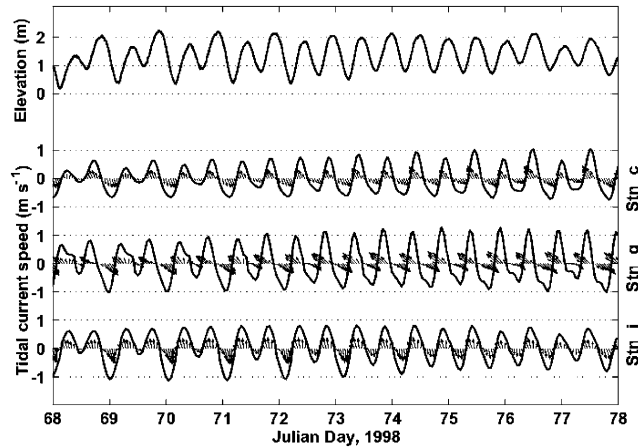


Fig. 10. Tidal currents predicted from dominant semi-diurnal M2 and S2 and dominant diurnal O1, K1 tidal ellipse parameters during the dry season in 1998. The top panel is for sea level variability. Flowing curves and vectors were predicted tidal current speeds (in m s^{-1}) and vectors for Stns c, g and j, respectively. Negative and positive current speeds indicate ebb and flood currents, respectively.

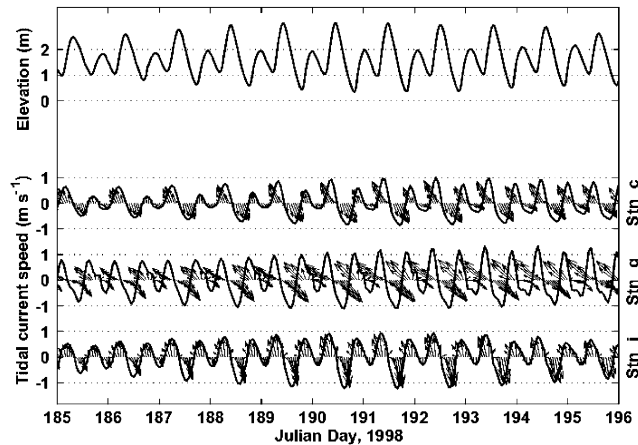


Fig. 11. Tidal currents predicted from dominant semi-diurnal M2 and S2 and dominant diurnal O1 and K1 tidal ellipse parameters during the wet season in 1998. The top panel is for sea level variability. Flowing curves and vectors were predicted tidal current speeds (in m s^{-1}) and vectors for Stns c, g and j, respectively. Negative and positive current speeds indicate ebb and flood currents, respectively.

tidal velocity was characterized by more intense flood than ebb currents, as an ebb flow with a longer ebb duration must be balanced by a shorter, more intense flood flow. But in the southeastern part of Lingdinyang (Stn j), the ebb flow was more intense than the flood flow. The flood and ebb flows lasted for a similar duration. Spectral energy

transfer is more pronounced in the velocity field with friction directly removing energy from the primary semi-diurnal constituent (Aubrey and Speer, 1985). This is in agreement with the tidal duration asymmetric analysis that the PRE is characterized by shorter, more intense flood than ebb currents (flood dominant). Due to a sea level

daily inequality, a tidal velocity daily inequality was also present in the PRE and in-phased with the sea level daily inequality.

4. Summary

The tides in the PRE are influenced by the complex delta formation, bottom topography, meteorology and river discharge when the tides propagate from offshore into the shallow estuary. Unlike other temperate estuaries, the average tidal range in the PRE increases gradually from the offshore region to the estuary, reaching a maximum at the head of the PRE (Humen) as the estuary becomes narrower and shallower, which concentrates the energy of the tides (Xu, 1985; Zhao, 1990). The friction and the non-linear transfer of energy, strongly delayed the phase of the tidal constituents. The amplitude increment of the main tidal constituents from offshore (Stn H) to the northern part of the estuary was also significant. However, the extent of the amplitude increment was different between diurnal constituents and semi-diurnal constituents. This could be illustrated from analyses of the temporal and spatial distribution of sea level variance. The percentage of SLV in the semi-diurnal band increased from offshore to the estuary, but it reversed for the diurnal band. The accentuated SLV in semi-diurnal band resulted in increased amplitudes of semi-diurnal constituents which were larger than diurnal constituents.

The main components of the current in the PRE were the river discharge, salt water intrusion and tidal currents. In the northern part of the PRE, the tidal currents were rectilinear, and the river discharge was dominant in non-tidal currents. At the western boundary of the PRE, the outflow due to the three river outlets was always stronger in the northwest than in the northeast, but the tidal currents were weaker in the northwest than in the northeast. Southeast of Lindingyang, the tidal currents were rotary and the river outflow dominated non-tidal currents in the top layer, while the salt water intrusion dominated in the lower layer. The current analysis indicated that in Lindingyang, freshwater outflow occurred via the

western channel, while the salt water intrusion occurred mainly via the eastern channel.

Acknowledgments

This work is part of the National Natural Science Foundation of China (# 40176006 and # 40376004).

References

- Andreas, M., 1998. Tidal currents in a topographically complex channel. *Continental Shelf Research* 18, 561–584.
- Aubrey, D.G., Speer, P.E., 1985. A study of non-linear tidal propagation in shallow inlet/estuarine systems. Part 1: observations. *Estuarine Coastal and Shelf Science* 21, 185–205.
- Denman, K.L., Powell, T.M., 1984. Effects of physical processes on planktonic ecosystems in the coastal ocean. *Oceanography and Marine Biology: An Annual Review* 22, 125–168.
- Foreman, M.G., 1978. Manual for tidal currents analysis and prediction. Pacific Marine Science Report 78-6, Institute of Ocean Sciences, Patricia Bay, Sidney, BC, Canada, p. 2.
- Friedrichs, C.T., Aubrey, D.G., 1988. Non-linear tidal distortion in shallow well-mixed estuaries: a synthesis. *Estuarine Coastal and Shelf Science* 27, 521–545.
- Hansen, D.V., Rattray, M.J., 1966. New dimensions in estuary classification. *Limnology and Oceanography* 11, 319–326.
- Leonard, W.H., 1976. The effect of the Spring-neap tidal cycle on the vertical salinity structure of the James, York and Rappahannock Rivers, Virginia, USA. *Estuarine Coastal Marine Science* 5, 485–496.
- Shaoling, H., Kot, S.C., 1997. Numerical model of tides in Pearl River Estuary with moving boundary. *Journal of Hydraulic Engineering* 123, 21–29.
- Speer, P.E., Aubrey, D.G., 1985. A study of non-linear tidal propagation in shallow inlet/estuarine systems. Part 2: theory. *Estuarine Coastal and Shelf Science* 21, 207–224.
- Xu, J.L., 1985. Shoal Growth and Evolution of Lindingyang of the Pearl River Mouth. China Ocean Press, Beijing (in Chinese).
- Ye, L., Preiffer, K.D., 0. Studies of 2D & 3D numerical simulation of Kelvin tide wave in Nei Lindingyang at Pearl River Estuary. *Ocean Engineering* 8 (4), 33–44.
- Yin, K., Harrison, P.J., Pond, S., Beamish, R.J., 1995a. Entrainment of nitrate in the Fraser River plume and its biological implications. I. Effects of salt wedge. *Estuarine Coastal and Shelf Science* 40, 505–528.
- Yin, K., Harrison, P.J., Pond, S., Beamish, R.J., 1995b. Entrainment of nitrate in the Fraser River plume and its biological implications. II. Effects of spring vs neap tides and river discharge. *Estuarine Coastal and Shelf Science* 40, 529–544.
- Zhao, H., 1990. The Evolution of the Pearl River Estuary. China Ocean Press, Beijing, pp. 1–357 (in Chinese).